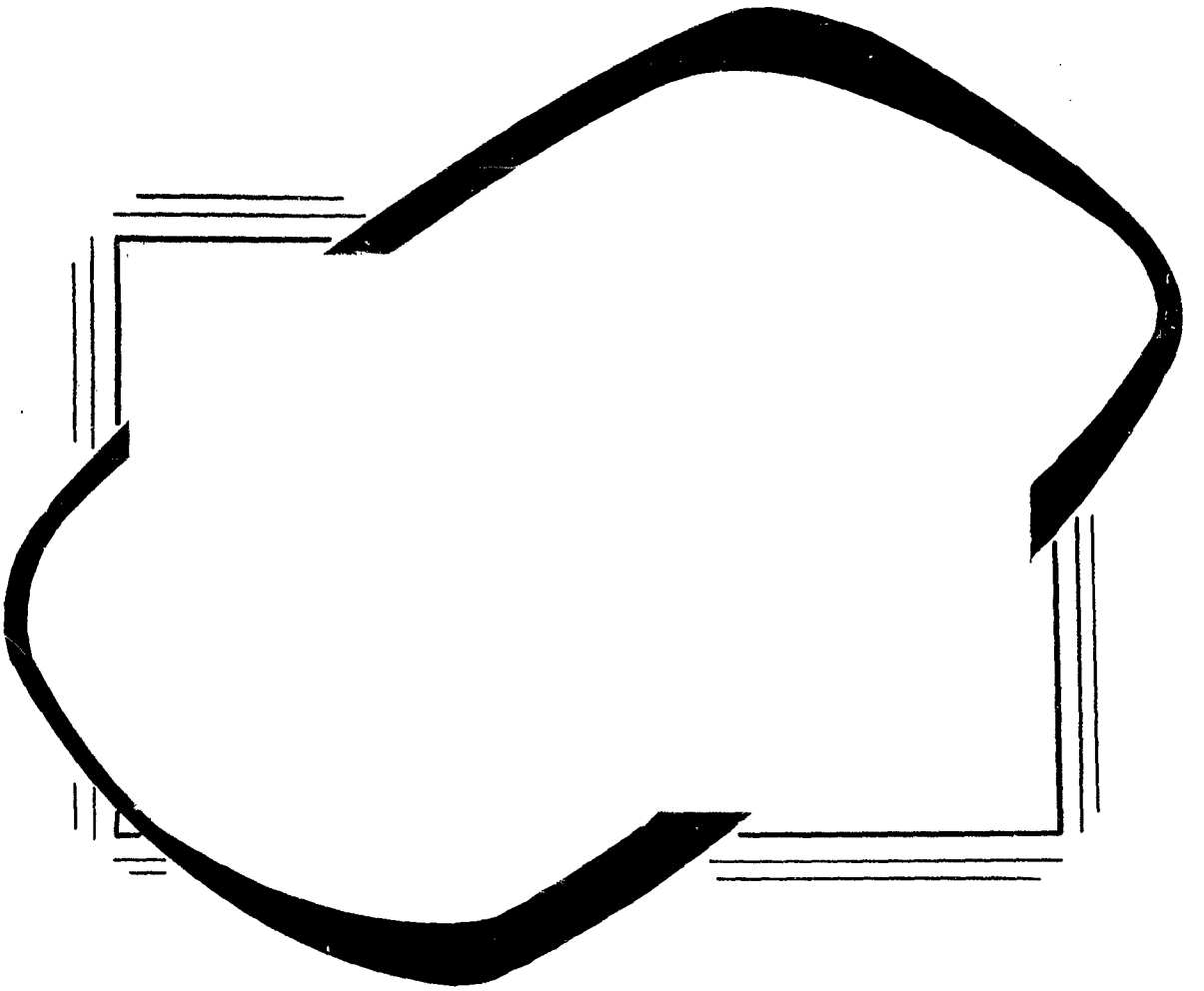

THE AEROPHYSICS DEPARTMENT Of MISSISSIPPI STATE UNIVERSITY

AN INVESTIGATION OF THE EFFECTS OF INDUCED NONSYMMETRIC PRESSURE DISTRIBUTIONS ON THE AERODYNAMIC STABILITY OF AN AIRSHIP FORM

By

Donald W. Boatwright

Research Report No. 36 11 August 1961

Conducted For
OFFICE OF NAVAL RESEARCH
Under
CONTRACT NONR 978 (02)

By

The Aerophysics Department
Mississippi State University

TABLE OF CONTENTS

LIST OF FIGURES

LIST OF SYMBOLS

x	Distance along longitudinal axis from nose	feet
L	Length of model	feet
r	Local radius	feet
t	Thickness of spoiler	feet or inches
R	Maximum radius of model	feet
h	Height of spoiler or bulge	feet or inches
s	Area of spoiler	square feet
V	Volume of model	cubic feet
C. B.	Position of center of buoyancy of ZS2G-1 airship	feet
δ_e	Elevator deflection	degrees
η_p	Propulsive efficiency of rotor	dimensionless
θ	Angle measured counter-clockwise from mid-position on port side of model	degrees
α	Angle of attack	degrees
Q	Flow quantity	cubic feet per minute
R_l	Reynolds number	dimensionless
U	Velocity	feet per second or knots
P	Static pressure	pounds per square foot
q	Dynamic pressure	pounds per square foot
C_L	Lift coefficient $= \frac{\text{Lift (lbs)}}{q_o V 2/3}$	dimensionless

C_D	Drag coefficient = $\frac{\text{Drag (lbs)}}{q_o V^{2/3}}$	dimensionless
C_M	Moment coefficient = $\frac{\text{Moment (ft-lbs)}}{q_o V}$	dimensionless
C_p	Pressure coefficient = $\frac{P - P_o}{q_o}$	dimensionless

Subscripts

p	Denotes forces or moments due to static pressure distribution
o	Denotes freestream conditions
R	Signifies conditions due to rotor

INTRODUCTION

The airship research program conducted by the Aerophysics Department of Mississippi State University has been directed toward improvement of the overall performance capabilities of the airship. Past research efforts have included full-scale boundary layer measurements on a ZS2G-1 airship and investigation of drag reduction by geometric modification of airship components. An analysis of experimental results and a study of drag breakdowns for various airship configurations have indicated that further improvement of airship performance may be gained from stern propulsion.

Since approximately 20 per cent of the overall drag of an airship may be attributed to fins, control surfaces, brace cables, and tail surface accessories, a large drag reduction would be realized by removal of these components. The drag breakdown for a finless, stern-propelled ZS2G-1 airship shows a drag reduction of 57 per cent compared to that of the conventional ZS2G-1. (Reference 1).

Partial control of the finless ZS2G-1 airship configuration (as suggested in Reference 1) would be available from cyclic pitch operation of the stern rotor. This report will demonstrate, however, that control moments available from a rotor cyclic pitch system are smaller than required by maneuverability criteria at low rotor thrust values. Consequently, removal of the fins of the airship presents a serious control problem, and necessitates development of other control systems which will act independently or in conjunction with the rotor system to supply the degree of control required. Such systems must also have low drag in a non-actuated condition.

Installations which would induce nonsymmetric pressure distributions about the airship hull or create high off-center drag forces were suggested for evaluation as possible control devices for the finless airship. (Reference 2). Inflatable, compartmented rings or bulges, and extensible spoilers are examples of the type of devices considered worthy of investigation.

This report contains the results of a study of the effects of induced nonsymmetric pressure distributions on the aerodynamic stability of an airship model as a first step toward the evaluation of such control devices. Flight test measurements of the pressure distributions of a ZS2G-1 model were integrated to obtain force and moment parameters acting on the model and were compared to conventional airship data. An analysis of the results using geometric devices and air ejection for inducing nonsymmetric pressure distributions are presented herein.

DESCRIPTION OF TESTS AND INSTRUMENTATION

Test Program

Pressure distributions were measured on a 13-foot fiberglas-plywood model of the ZS2G-1 airship. The model was mounted above an AT-11 aircraft on an adjustable strut arrangement as shown in Figure 3. Phases of the test program were as follows:

1. Preliminary Flow Measurements Above the Aircraft
   Measurements made prior to installation of the model to examine the static pressure and velocity field in the region to be occupied by the model.
2. Pressure Distributions About the Bare Hull
   Measurements made on the bare hull to determine the degree of instability of the model at angles of attack.
3. Pressure Distributions Using Plywood Spoilers
   An investigation of the effect of a simple geometric device on model stability.
4. Pressure Distributions Using a Sinusoidal Bulge
   To determine the effect of a large geometric change of body shape on stability.
5. Pressure Distributions Using Air Ejection Through a Slot in the Nose of the Model.
   To investigate a non-geometrical means of stabilization.

Test Conditions

Since the model was to be mounted near the aircraft, it was necessary to examine the flow field in the region to be occupied by the model. A survey of the region was made for a series of flight conditions to determine the static and dynamic pressure variations as well as streamline deviation relative to the freestream flow. This information allowed data to be corrected for errors due to the proximity to the aircraft. Corrected data were compared to theoretical and wind tunnel data and found to agree within acceptable limits. Comparison of experimental and theoretical pressure distributions are shown in Figure 6.

The model was mounted on adjustable struts to allow angle of attack to be changed within $\pm$ 15 degree limits. No arrangement was made to yaw the model since yaw conditions could be simulated by change in angle of attack of the symmetrical model. Angle of attack and zero yaw conditions were maintained in flight by use of the aircraft angle of attack indicator as well as balanced static pressure readings from orifices located at the nose of the model. Airspeed was measured on a calibrated indicator using a trailing static pressure sonde for freestream static pressure reference.

ZS2G-1 Model and Test Devices

The ZS2G-1 model construction consisted of a series of internal plywood bulkheads which were bonded to the Fiberglas hull. The hull was sanded to a smooth finish and several coats of lacquer applied. Additional sandings resulted in an exceptionally smooth and wave-free surface.

Model Dimensions

Length	12.64 feet
Volume	58.70 cubic feet
Wetted Area	95.05 square feet
Scale	1/22.3
Center of Buoyancy Position	5.78 feet from nose
Maximum Diameter	3.028 feet
L/D Ratio	4.175
$(\text{Volume})^{1/3}$	3.886 feet
$(\text{Volume})^{2/3}$	15.12 square feet

Distance of the longitudinal axis of the model from the aircraft at zero angle of attack was 4.0 feet. Coordinates of the model are plotted in Figure 1.

Description of Spoiler and Bulge Devices

Four plywood spoilers and a sinusoidal bulge were used during the test program to induce nonsymmetric pressure conditions about the model. Spoilers were designed for attachment to the body at four positions relative to body length and to act on one quadrant of the model. Thus, the circumferential span of each spoiler was 0.25 times the model circumference at each location. Spoilers were 2.5 inches high and 0.25 inch thick. A typical spoiler is illustrated in Figure 4.

Spoiler Attachment Positions and Areas

1. x/L = 0.0722	A = 0.327	square feet
2. x/L = 0.1687	A = 0.451	square feet
3. x/L = 0.2653	A = 0.505	square feet
4. x/L = 0.3730	A = 0.529	square feet

A Fiberglas bulge was the second geometric device tested. The outside bulge shape was that of a sine curve faired into the body curvature at stations x/L = 0.026 and x/L = 0.112. Maximum thickness of the model at the bulge section was located at x/L = 0.0722. Height of the bulge was 2.5 inches at this position. Figure 5 shows the bulge installed on the model.

Blower System for Air Ejection

Figure 4 shows a photograph of a slot in the nose of the model through which air was ejected from a blower within the aircraft. The system consisted of an intake scoop located beneath the aircraft, a calibrated venturi, and a blower capable of delivering 350 cubic feet of air per minute. The venturi was used to determine flow volume through the system.

A flexible tube, 4 inches in diameter, connected the blower to the model. Internal plywood flow guides were installed to eject air normal to the model surface. Slot length was 0.25 times model circumference. Figure 4 shows a slot 0.1875 inch wide at x/L = 0.182.

Instrumentation

An adjustable yaw head and a rake of static and total pressure-measuring tubes were used in the flow survey above the aircraft.

All pressure distributions were measured at constant dynamic head which was read from a calibrated pressure indicator. Freestream total pressure was measured by use of a Kiel tube mounted at the nose of the aircraft. Freestream static pressure was obtained from a calibrated sonde which was lowered from the aircraft by a thin wire cable.

A panel of 24 pressure indicators was used for measurements of pressure distribution over the model surface. Since a large number of measurements were required for each pressure survey, it was necessary to install a plug-in type switching panel between the instruments and model. The instrument panel also held two airspeed indicators which were used to indicate angle of attack and yaw.

The upper half of the model was equipped with 137 flush-mounted orifices which were connected to the interior of the aircraft by 0.125 inch plastic tubing. These orifices were arranged in circumferential rows 22.5 degrees apart. Four additional rows were installed on the lower half of the model to aid in checking agreement of data at zero angle of attack.

Only the upper half of the model was used for measurements in order to minimize errors due to the supporting struts. This procedure required measurements on the upper surface at negative angles of attack for simulation of conditions on the lower half of the model at corresponding positive angles of attack.

Pressure distributions about the spoilers and bulge were obtained using small, flat pressure-measuring tubes and flush surface orifices.

REDUCTION OF DATA

Pressure distributions were integrated graphically to determine pressure drag, lift, and moments about station $x/L = 0.4574$. This station corresponds to the center of buoyancy position of the ZS2G-1 airship and was chosen for convenience of data comparison with the full-scale airship.

The graphical method of obtaining forces and moments acting on a body is commonly used, although subject to error unless pressure distributions are carefully measured and a sufficient number of points along the body are included in the calculations. In preparing this report efforts were made to reduce error to a minimum.

The model surface was divided into 16 longitudinal sections along which pressure distributions were measured. Integration of the static pressure acting on each section and a summation of results were taken to obtain forces and moments acting on the entire model. A total of 42 points along each section was used in the calculations.

Special attention was given to the nose section of the model where errors were most likely to occur. A final comparison of results revealed some data scatter, but fair agreement was noted with previously measured wind tunnel data.

Equations used for graphical integration of the static pressure distributions about the model may be expressed in the following general forms:

1. Force coefficient parallel to longitudinal axis

$$C_{A_p} = \frac{2\pi}{V^{2/3}} \left[\int_{r_{x=0}}^{R} C_p \, r \, dr - \int_{R}^{r_{x=L}} C_p \, r \, dr \right]$$

2. Force coefficient normal to longitudinal axis

$$C_{N_p} = \sum_{1}^{16} \frac{\pi}{8V^{2/3}} \int_{0}^{L} - C_p \, r \sin\theta \, dx$$

$\sum$ indicates summation of forces on 16 longitudinal body sections.

3. Moment coefficient about position of maximum thickness due to force parallel to longitudinal axis

$$C_{M_{A_p}} = \sum_{1}^{16} \frac{\pi}{8V} \left[\int_{r_{x=0}}^{R} C_p \, r^2 \sin\theta \, dr - \int_{R}^{r_{x=L}} C_p \, r^2 \sin\theta \, dr \right]$$

4. Moment coefficient about position of maximum thickness due to force normal to longitudinal axis

$$C_{M_{N_p}} = \sum_{1}^{16} \frac{\pi}{8V} \left[\int_{0}^{x_{r=R}} C_p \, rx \cos\theta \, dx - \int_{x_{r=R}}^{L} C_p \, rx \cos x\theta \, dx \right]$$

5. Pressure drag coefficient at an angle of attack

$$C_{D_p} = C_{A_p} \cos\alpha + C_{N_p} \sin\alpha$$

6. Lift coefficient at an angle of attack

$$C_{L_p} = C_{N_p} \cos \alpha - C_{A_p} \sin \alpha$$

7. Total moment coefficient about position of maximum thickness

$$C_{M_p} = C_{M_{A_p}} + C_{M_{N_p}}$$

C_{M_p} was transferred to the C. B. position for comparison to airship data. (See Figure 2 for notation).

DISCUSSION OF RESULTS

A spoiler or bulge, installed near the nose of a symmetrical body of revolution at zero angle of attack, will cause nonsymmetry of the static pressure distribution about the body. Near the location of a bulge, for example, static pressure becomes more negative due to acceleration of the flow, or "supervelocity." A destablizing moment arises as a result of the nonsymmetric distribution of static pressure forces along the surface of the body which tends to rotate the body from its original position. When the body is at an angle of attack, however, induced moments may be either stabilizing or destabilizing, depending upon the particular type of device used and its effects on the flow about the body.

The current work attempts to determine the effects of induced nonsymmetric pressure distributions on stability of a finless airship form. Final results are compared to conventional airship data, and the devices used are evaluated as possible control units for the stern-propelled airship.

During this investigation, graphical integration was used to determine moments about the center of buoyancy position due to static pressure forces only. Moments resulting from off-center forces arising from frictional drag were not included in analysis of the current problem. Moments due to drag forces are generally small in the present situation, however, and neglect of frictional drag moments should not seriously affect final results.

Pressure Distribution Characteristics

Pressure distributions are illustrated in Figure 6 which allow comparison of model tests with theoretical and previously measured wind tunnel data. Figures 7, 8, and 9, show pressure distributions as affected by the test devices at zero angle of attack.

Some correlation between moment about the center of buoyancy position and characteristics of the pressure distribution may be noted from these plots. The bulge device produces a large, negative pressure peak, but also creates a high, positive pressure region immediately behind its location on the model. This high pressure region tends to cancel the nose-up moment resulting from the negative pressure peak when the bulge is located on the upper nose section.

A similar situation exists when a spoiler is used. A high pressure region exists some distance aft of the spoiler, which is less pronounced than that which occurs behind the bulge. However, this region plus the stagnation pressure region at the base of the spoiler reduce the nose-up moment resulting from the negative pressure peak which occurs immediately behind the spoiler.

The above effects, combined with drag characteristics, determine the total nose-up pitching moment produced by each device. The spoiler produced the higher nose-up moment, primarily because of its higher drag rather than its effect on lift.

Tests with air ejection were limited in number because of termination of the project, and since air ejection from a single slot did not appear attractive at the flow quantities available for the tests. Nose-up pitching moment resulting from this method was generally due to higher pressures on the rear of the model rather than from effects at the nose. (Figure 9).

Pressure recovery at the rear of the model remained essentially constant for all test conditions. Some scatter of data occurred because of highly turbulent flow generated by the test devices and, consequently, some inconsistency was noted in final results. The data, however, were sufficiently accurate to indicate the general magnitude of the moments produced by each device.

Effect of Spoiler Location

Pressure distributions were measured with spoilers attached at four positions along the length of the model. These tests were conducted to determine the magnitude of moments produced by the spoilers relative to location of the minimum pressure point on the bare hull. Results are illustrated in Figure 10.

It is interesting to note that pressure drag of the model is maximum at the point of minimum pressure. Lift, however, varies considerably with spoiler location, being maximum a short distance behind the minimum pressure point. Maximum moment occurred at the most forward spoiler location, primarily because of the greater distance to the center of buoyancy rather than from higher lift at this position. Negative moment coefficients occurred when the lift vector was shifted aft of the center of buoyancy.

These measurements indicate that effectiveness of a control device is strongly dependent upon location of the device relative to the point of minimum pressure and distance from the center of buoyancy of the airship.

Spoiler and Bulge Tests at an Angle of Attack

Tests with a spoiler and bulge were made at angles of attack with devices located on the upper and lower quadrants of the model. Both devices were located at the most effective spoiler position determined from the previous tests. ($x/L = 0.0722$). Maximum height of the bulge, measured perpendicular to the longitudinal axis, was 2.5 inches which corresponded to spoiler height. Length was 8.5 per cent of the total length of the model.

Lift and pressure drag coefficients for the various bulge and spoiler arrangements are plotted in Figures 11 and 12. It will be observed that drag coefficients are negative in sign with the spoiler or bulge located on the lower model quadrant. The negative sign occurs since the normal force coefficient (C_{N_p}) is negative at positive angles of attack due to high negative lift of the spoiler and bulge.

Pressure drag due to the spoiler was larger than that of the bulge at small angles of attack. However, pressure drag at higher angles of attack varied with upper and lower location of each device.

Determination of lift coefficients of the model with both spoiler and bulge produced several unexpected results. The bulge, when located on the upper model quadrant, produced a negative lift coefficient at zero angle of attack which was opposite to that due to the spoiler. Furthermore, data show a negative increase of lift coefficient with increasing positive angle of attack for both devices located in the lower quadrant position.

Effect of Spoiler and Bulge on Model Stability

Moment coefficients about the center of buoyancy position due to lift and pressure drag are plotted in Figure 13. Moments were more positive than those of the bare hull when devices were located on the underside of the model at high angles of attack. Also, moment produced by the upper-mounted bulge was smaller than that of the bare hull. These results were surprising, but become evident upon inspection of the pressure distributions for the particular cases mentioned.

The spoiler, or bulge, when mounted on the upper model quadrant, produces a negative pressure peak which causes rotation of the model in a nose-up direction. However, flow separation induced by the device causes the pressure on the upper, rear portion of the body to become more negative which shifts the lift vector closer to the center of buoyancy position as angle of attack is increased. Nose-up moment due to lift therefore decreases, and in some instances, may be less than that of the bare hull.

High positive moments due to the lower-mounted spoiler and bulge at an angle of attack may be attributed to two effects. As angle of attack is increased, the negative moment due to drag of the device becomes more positive since the length of the moment arm with respect to the center of buoyancy position is reduced. In addition, increased negative pressure on the lower, rear portion of the model, due to accelerated flow over the test device, produces a high nose-up pitching moment. As a result, total nose-up pitching moment is larger when devices are located on the underside of the nose.

These results indicate that a lower-mounted spoiler control device for an airship would produce only small stabilizing moments at low positive angles of attack. The bulge-type control device appears to offer better possibilities as a control unit since it tends to produce a larger stabilizing effect at higher angles of attack.

Magnitude of moments produced by either spoiler or bulge is small, however, and neither appear sufficiently effective for use as control devices for an airship - even when used to supplement control available from a stern-propulsion unit.

Control Available from a Stern Rotor

Using values of total drag coefficient for the ZS2G-1 airship from Reference 3, moments available from a stern-propulsion unit of an advanced, finless ZS2G-1 airship configuration were computed for various airspeeds and angles of attack. (Figure 14). Drag coefficients of the original airship were reduced by 57 per cent as an approximation of the drag coefficients of the advanced airship configuration. (Refer to Reference 1).

A maximum airspeed of 100 knots and a rotor propulsive efficiency of 67.5 per cent were assumed in the calculations. A power plant capable of delivering approximately 1500 horsepower to the rotor is required to drive the airship at a maximum velocity of 100 knots. Control moments available from cyclic pitch control were computed for a rotor tilt of 15 degrees with respect to the longitudinal axis of the airship.

Figure 14 illustrates the magnitude of the control moments available from the stern-propulsion unit at maximum airspeed and full

rotor thrust conditions. It will be noted that the rotor is capable of producing only a small fraction of the moment required to overcome instability of the bare hull for the above flight conditions.

Marginal control of the airship appears possible, however, with application of full power at low flight velocities. Calculations show that the rotor will produce a stabilizing moment at an angle of attack of 15 degrees, providing airspeed is below about 13.5 knots. Airspeed is therefore seriously restricted when cyclic pitch control of the stern rotor is the only means of control available for a finless-type airship.

Discussion of a Combined Control System

Tests with the spoiler and bulge devices indicate the upper, nose-mounted bulge to be the more effective device for reducing the destabilizing moment of the bare hull. Figure 15 shows the degree of stability possessed by a finless, stern-propelled airship having cyclic pitch control of the rotor combined with a bulge-type control device at the nose. Two conditions are illustrated: (1) steady flight conditions at maximum rotor thrust and maximum airspeed, and (2) maximum rotor thrust at a lower flight velocity. The latter case assumes full power application to the rotor at an airspeed 30 knots.

Under condition one, at maximum velocity, the airship would be unstable at all angles of attack. Condition two shows that control of the airship would not be possible above an airspeed of 30 knots at 10 degrees angle of attack.

A comparison of the combined bulge and rotor system with the XZP5-K airship is made in Figure 16. These curves show that the bulge rotor system at maximum rotor thrust and maximum airspeed will offer

only slightly higher stabilization to the airship than is presently possessed by the XZP5-K with fins at zero elevator deflection. At an airspeed of 30 knots, stabilizing moments produced by the bulge-rotor system are comparable to the XZP5-K with elevators deflected - 10 degrees.

These curves are also compared with the airship having an elevator deflection of -30 degrees. Moment coefficient of the XZP5-K for this condition is approximately 2.5 times larger than that of the stern-propelled airship at 30 knots.

Projected Research

Final results indicate the bulge-rotor system to be relatively poor as a means for controlling the finless-type airship. The possibility exists, however, that such systems may be perfected through future research efforts and prove applicable to vehicles aerodynamically similar to the airship.

Torpedoes, for example, present control problems not unlike those of the finless airship since the torpedo is a stern-propelled vehicle having restricted control surface area. Fluid ejection systems for torpedoes are currently being evaluated by various research agencies in an effort to solve the torpedo problem. Other concepts, such as the use of geometry-changing devices, may prove applicable to torpedo-type missiles, provided continued research is devoted toward perfection of required techniques.

Future development of low-drag control systems is essential in view of the ever-increasing demands for higher-speed, longer-range vehicles of all types.

CONCLUDING REMARKS

1. Control moments available from cyclic pitch operation of a proposed stern rotor are insufficient to provide stabilization of a finless airship at a full-power, maximum airspeed condition.
2. Control by cyclic pitch of a stern rotor is marginal at low airspeed with application of full power to the rotor.
3. Combination of a bulge-type control device with cyclic pitch control of a stern rotor does not appear applicable for airships because of restricted airspeed at moderate angles of attack.
4. A bulge-type control device used to supplement cyclic pitch control of the stern rotor produces a stabilizing influence to the finless airship comparable to that of a conventional airship with zero elevator deflection.
5. Tests indicate that the magnitude and direction of moments resulting from a spoiler or bulge device located on the forward portion of an airship form are strongly related to position of the device with respect to location of minimum pressure on the bare hull.
6. A bulge-type device is capable of producing a larger stabilizing effect on a finless airship form at moderate angles of attack than a spoiler of the same height and span.

REFERENCES

1. Cornish, J. J., III, and Boatwright, D. W. Application of Full-Scale Boundary Layer Measurements to Drag Reduction of Airships. (Aerophysics Department, Mississippi State University, Research Report No. 28), 18 January 1960. (Confidential).

2. Boatwright, D. W. A Research Proposal for a Study of Means for Inducing Non-Symmetric Pressure Distributions on an Airship Form. (Aerophysics Department, Mississippi State University, Unpublished Report), 12 April 1960.

3. Preliminary Performance Estimate for the XZS2G-1 and ZS2G-1 Airships. (Goodyear Aircraft Corporation, Akron, Ohio, Report No. 5268), 1 May 1953. (Confidential).

4. Cerreta, Peter A. Wind-Tunnel Investigation of the Drag of a Proposed Boundary-Layer Controlled Airship. (David Taylor Model Basin Aero Report No. 914), March 1957. (Confidential).

5. Young, A. D., and Owen, P. R. A Simplified Theory for Streamline Bodies of Revolution and Its Application to the Development of High-Speed Low-Drag Shapes. (Ministry of Supply RM No. 2071, London, England), July, 1943.

FIGURE 1

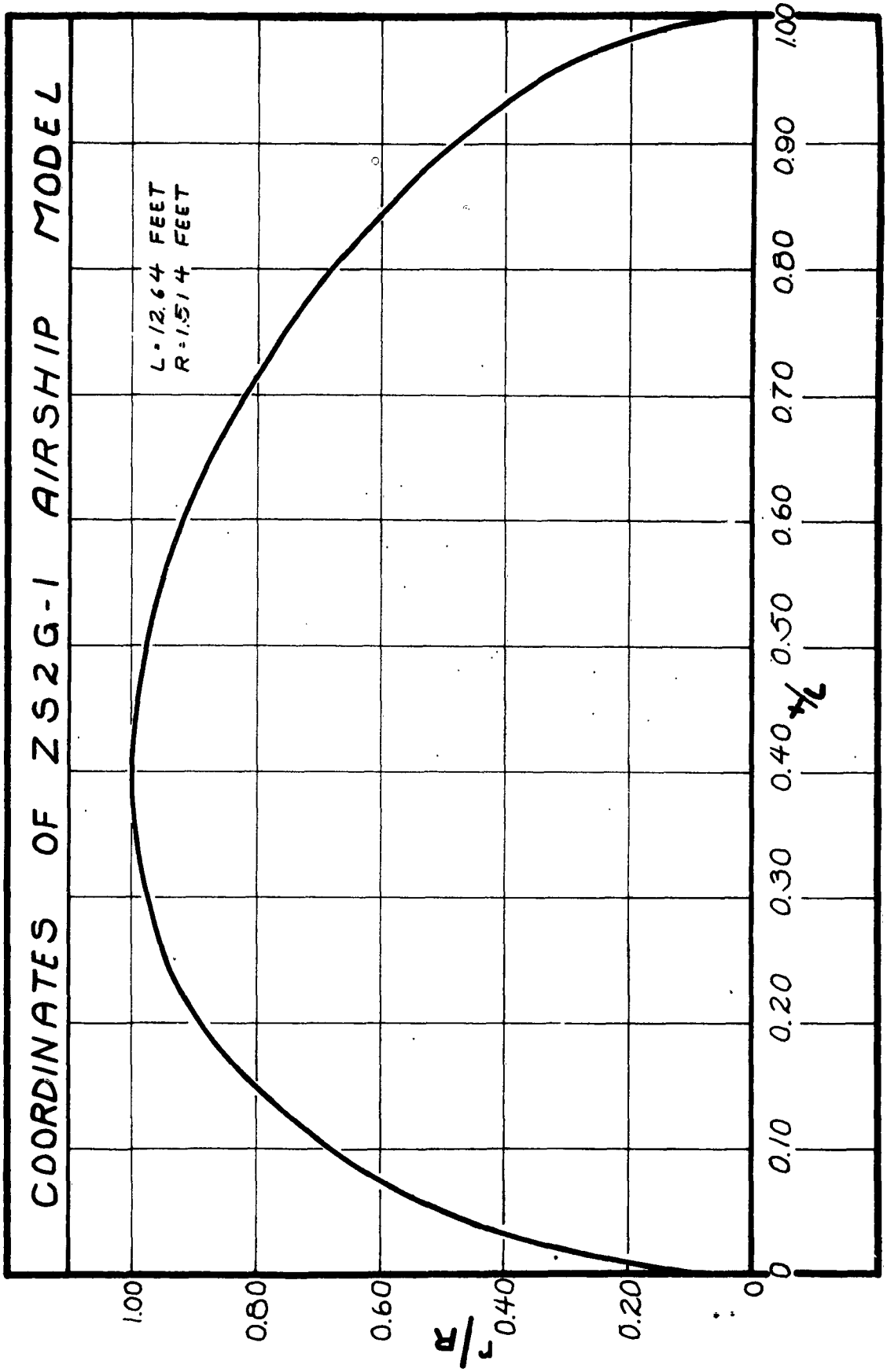
COORDINATES OF ZSG-1 AIRSHIP MODEL
L=12.64 FEET
R=1.514 FEET
r/R
x/L
0
0.20
0.40
0.60
0.80
1.00
0.10
0.30
0.50
0.70
0.90

FIGURE 2

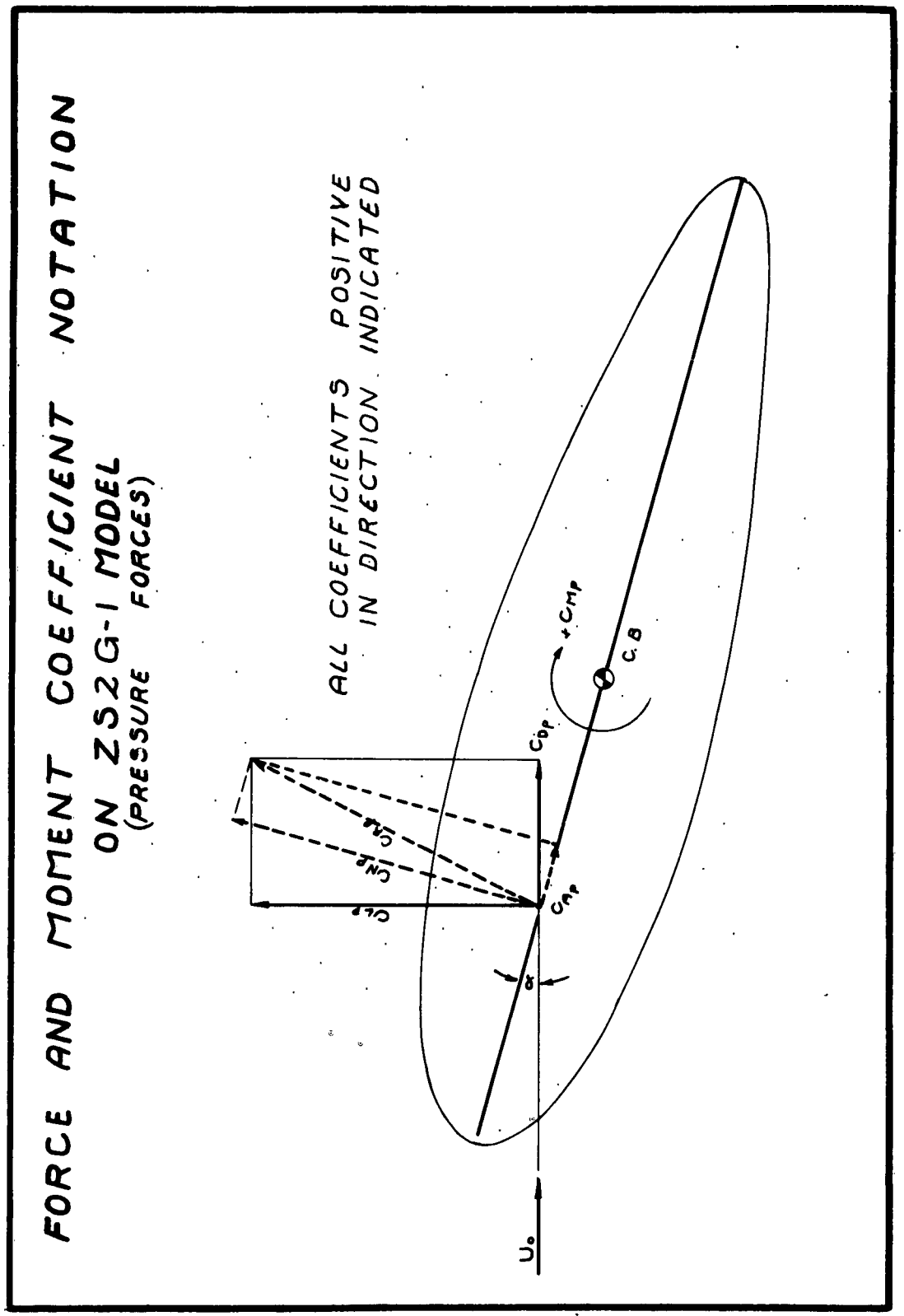
FORCE AND MOMENT COEFFICIENT NOTATION
ON ZS2G-1 MODEL
(PRESSURE FORCES)
ALL COEFFICIENTS POSITIVE
IN DIRECTION INDICATED
+CMP
C.G
CDP
CNP
CAP
CLP
α
U∞

FIGURE 3

PHOTOGRAPH OF AIRCRAFT WITH ZS2G-1 MODEL INSTALLATION

FIGURE 4

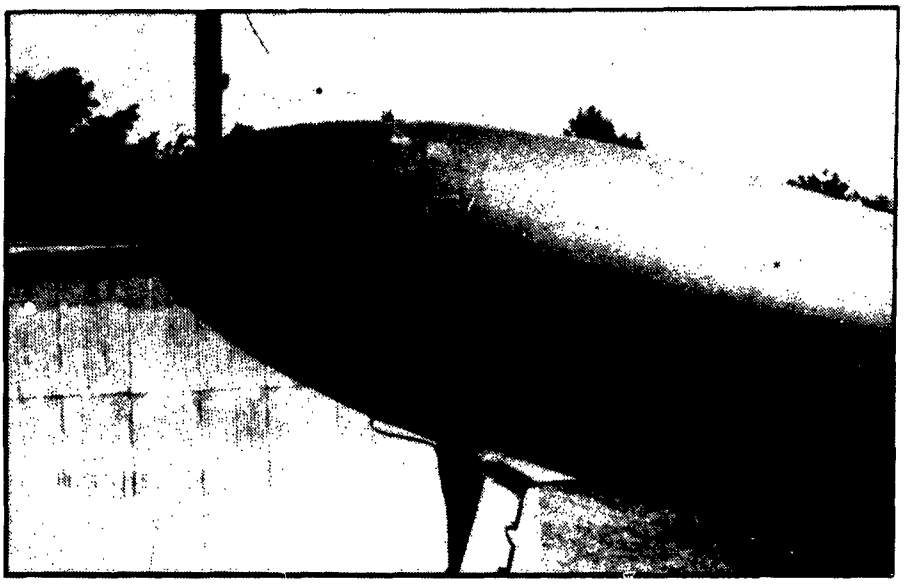

ZS2G-1 MODEL WITH SLOT FOR AIR EJECTION TESTS

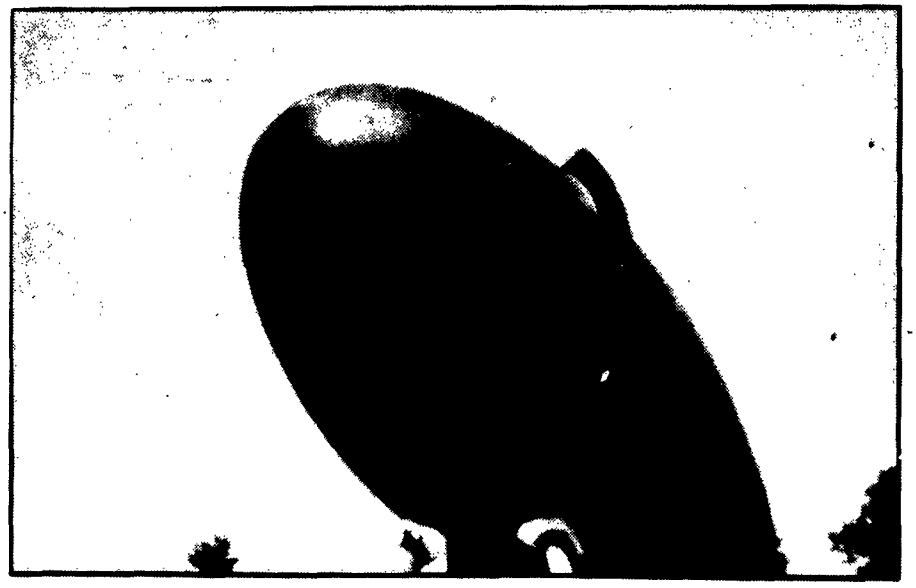

ZS2G-1 MODEL WITH SPOILER

FIGURE 5

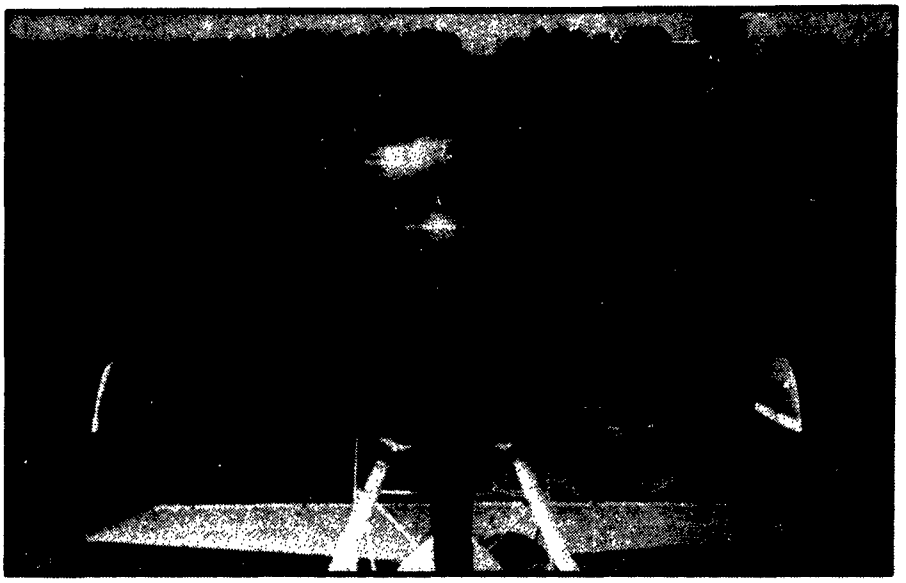

FRONT VIEW OF MODEL WITH BULGE INSTALLATION

SIDE VIEW OF MODEL WITH BULGE INSTALLATION

FIGURE 6

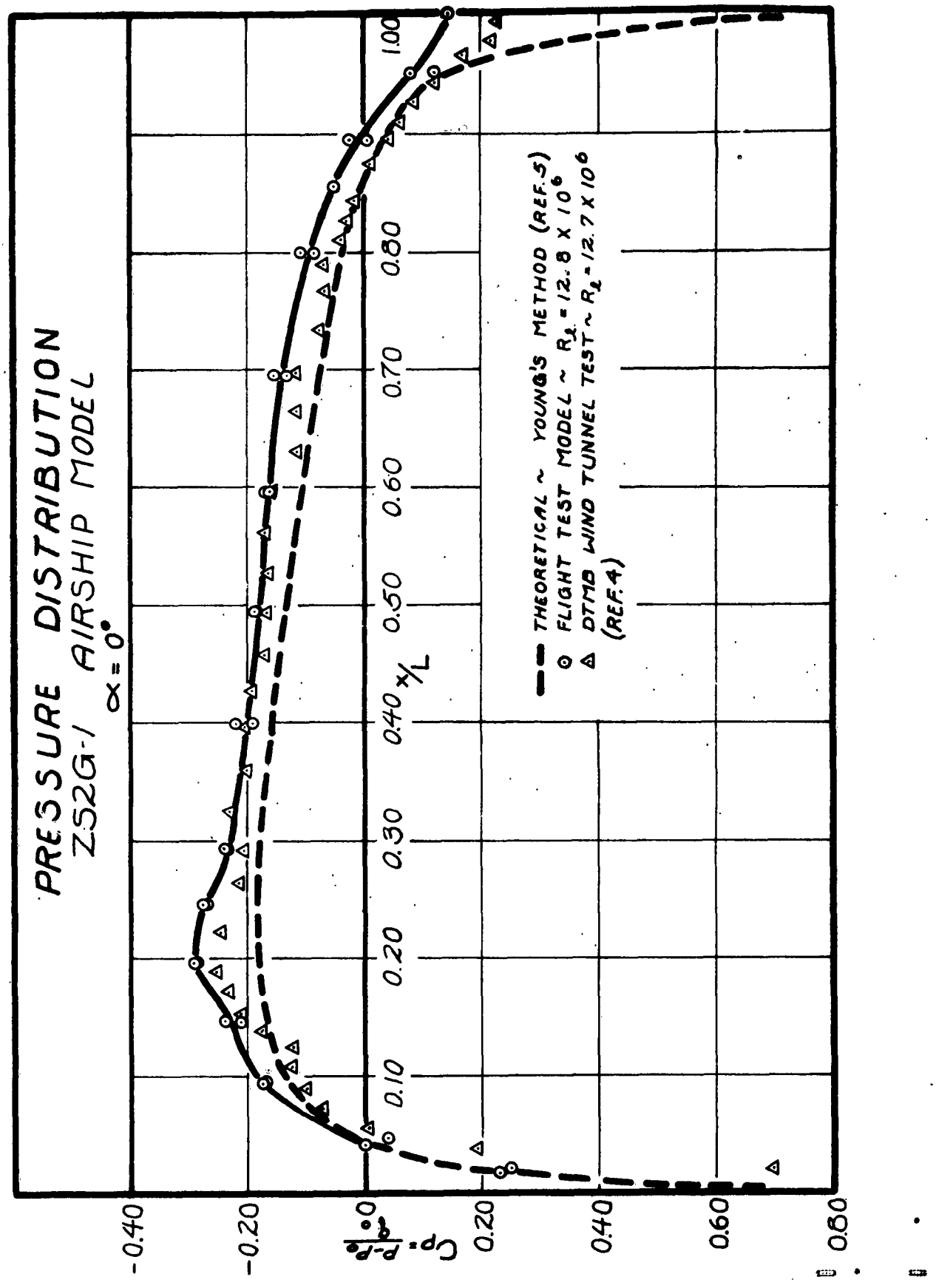
PRESSURE DISTRIBUTION
ZSZG-1 AIRSHIP MODEL
α = 0°
THEORETICAL ~ YOUNG'S METHOD (REF.5)
FLIGHT TEST MODEL ~ R_L = 12.8 X 10⁶
DTMB WIND TUNNEL TEST ~ R_L = 12.7 X 10⁶ (REF.4)
$C_p = \frac{p-p_0}{q_0}$
x/L
-0.40
-0.20
0.0
0.20
0.40
0.60
0.10
0.20
0.30
0.40
0.50
0.60
0.70
0.80
1.00

FIGURE 7

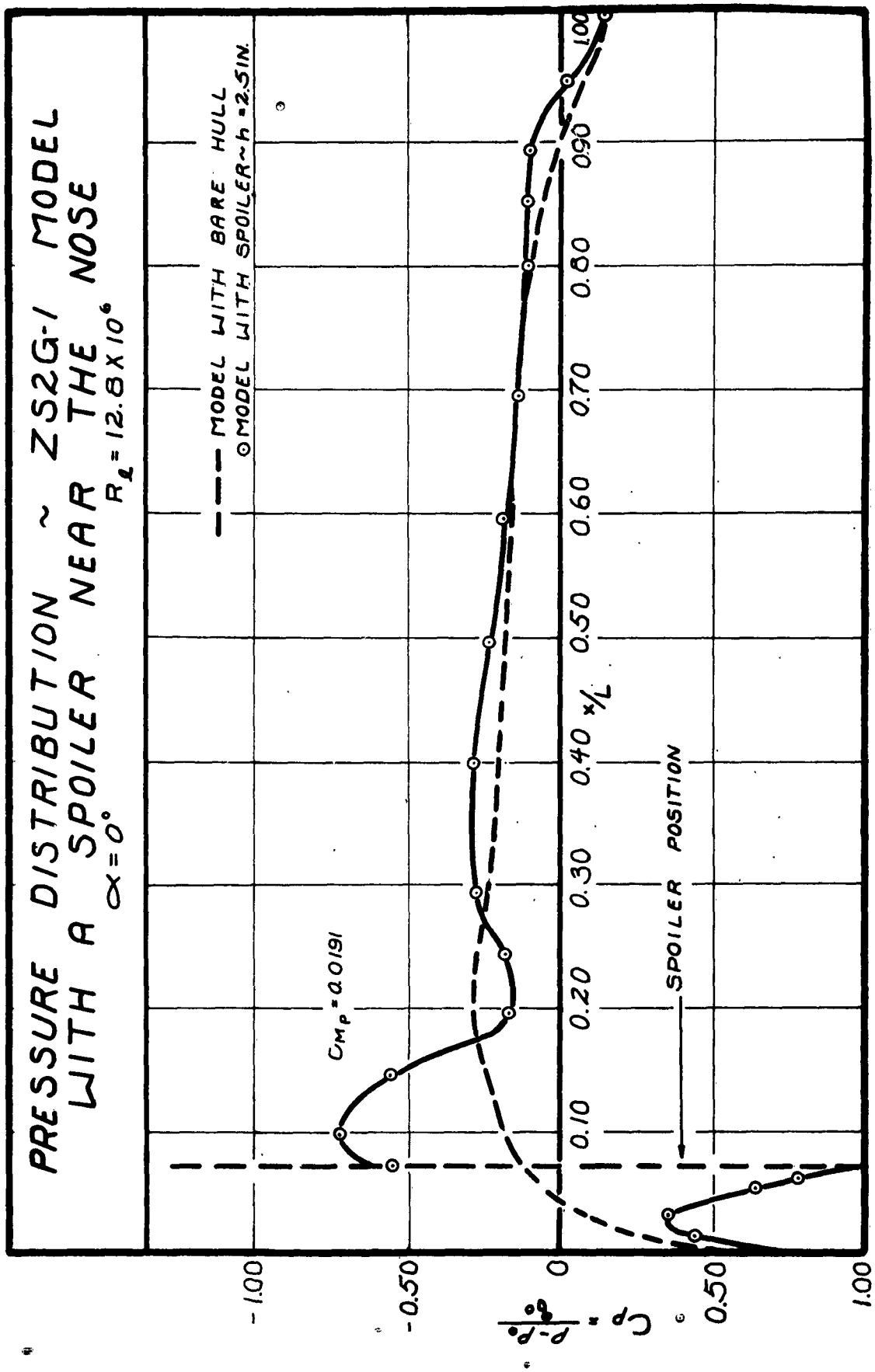
PRESSURE DISTRIBUTION ~ ZS2G-1 MODEL
WITH A SPOILER NEAR THE NOSE
$\alpha = 0°$
$R_L = 12.8 \times 10^6$
MODEL WITH BARE HULL
MODEL WITH SPOILER~h = 2.5IN.
$C_{M_P} = .0191$
SPOILER POSITION
$C_p = \frac{p - p_\infty}{q_\infty}$
x/L
-1.00
-0.50
0
0.50
1.00
0.10
0.20
0.30
0.40
0.50
0.60
0.70
0.80
0.90
1.00

FIGURE 8

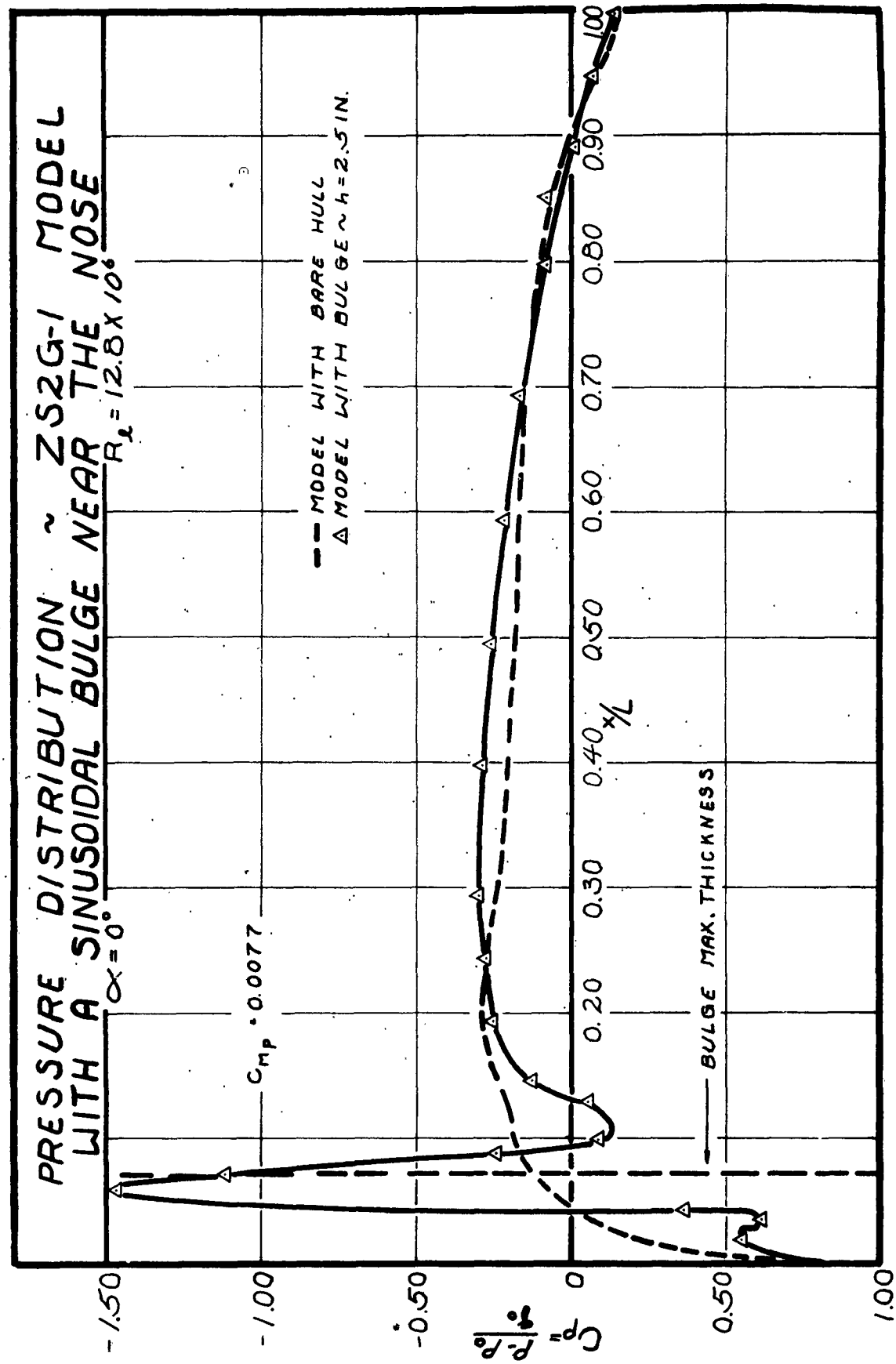
PRESSURE DISTRIBUTION ~ ZS2G-1 MODEL
WITH A SINUSOIDAL BULGE NEAR THE NOSE
$R_L = 12.8 \times 10^6$
$\alpha = 0°$
$C_{m_p} = 0.0077$
MODEL WITH BARE HULL
MODEL WITH BULGE ~ h = 2.5 IN.
BULGE MAX. THICKNESS
$C_p = \frac{p - p_\infty}{q_\infty}$
x/L
-1.50
-1.00
-0.50
0
0.50
1.00
0.20
0.30
0.40
0.50
0.60
0.70
0.80
0.90
100

FIGURE 9

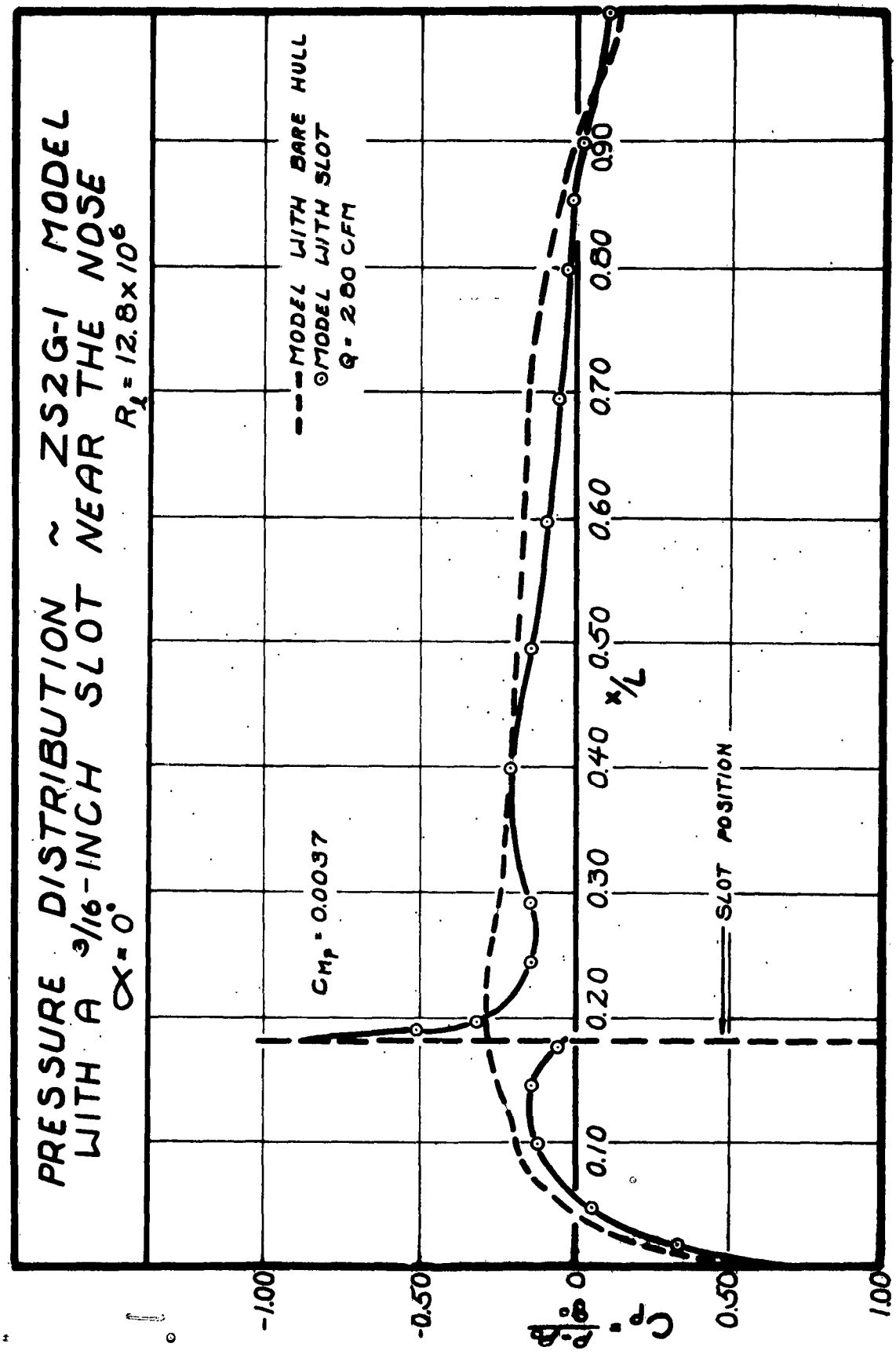
PRESSURE DISTRIBUTION ~ ZS2G-1 MODEL
WITH A 3/16-INCH SLOT NEAR THE NOSE
α = 0°
R_L = 12.8 x 10^6
MODEL WITH BARE HULL
MODEL WITH SLOT
Q = 2.80 CFM
C_mp = 0.0037
SLOT POSITION
x/L
0.10
0.20
0.30
0.40
0.50
0.60
0.70
0.80
0.90
-1.00
-0.50
0
0.50
1.00
C_p = (p - p_∞)/q_∞

FIGURE 10

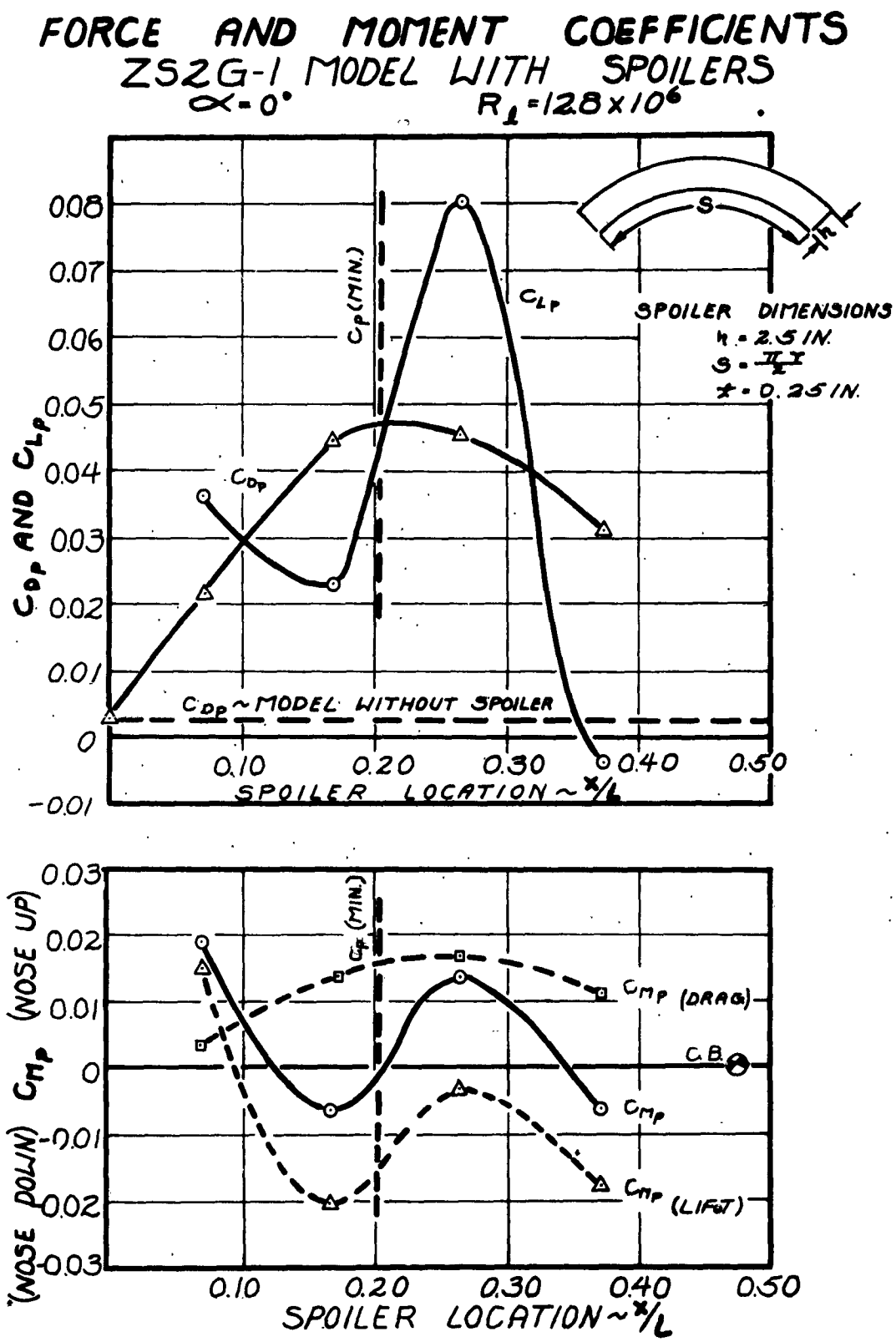
FORCE AND MOMENT COEFFICIENTS
ZS2G-1 MODEL WITH SPOILERS
α = 0°
R_l = 12.8 x 10^6
0.08
0.07
0.06
0.05
0.04
0.03
0.02
0.01
0
-0.01
C_Dp AND C_Lp
C_p (MIN.)
C_Lp
C_Dp
C_Dp ~ MODEL WITHOUT SPOILER
SPOILER DIMENSIONS
h = 2.5 IN.
s = πl/2
t = 0.25 IN.
s
h
t
0.10
0.20
0.30
0.40
0.50
SPOILER LOCATION ~ x/l
0.03
0.02
0.01
0
-0.01
-0.02
-0.03
(NOSE UP) C_mp (NOSE DOWN)
C_mp (MIN.)
C_mp (DRAG)
C.B.
C_mp
C_mp (LIFT)
0.10
0.20
0.30
0.40
0.50
SPOILER LOCATION ~ x/l

FIGURE 11

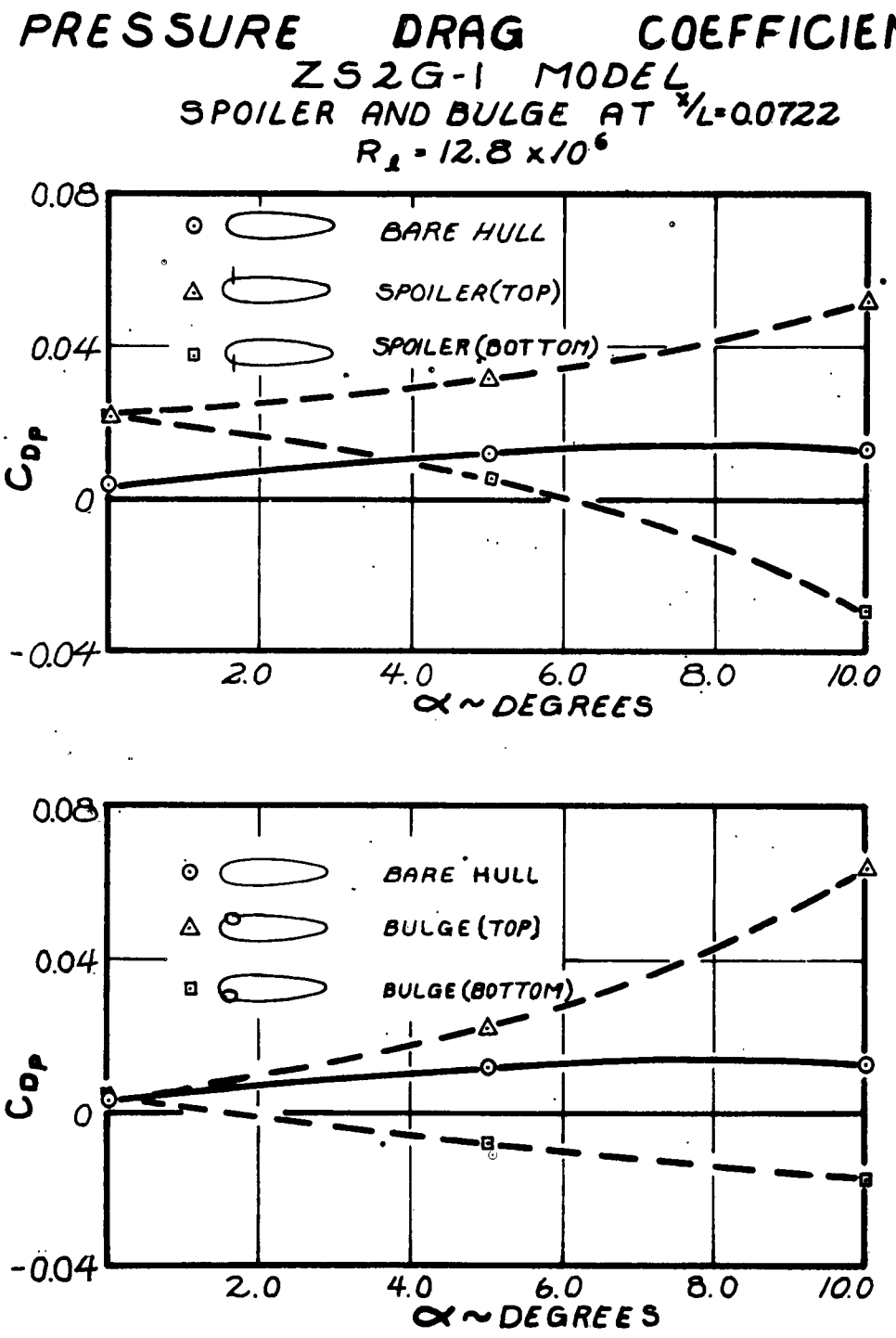
PRESSURE DRAG COEFFICIENT
ZS2G-1 MODEL
SPOILER AND BULGE AT X/L=0.0722
$R_L = 12.8 \times 10^6$
0.08
0.04
0
-0.04
C_{DP}
BARE HULL
SPOILER(TOP)
SPOILER(BOTTOM)
2.0
4.0
6.0
8.0
10.0
α ~ DEGREES
BARE HULL
BULGE(TOP)
BULGE(BOTTOM)

FIGURE 12

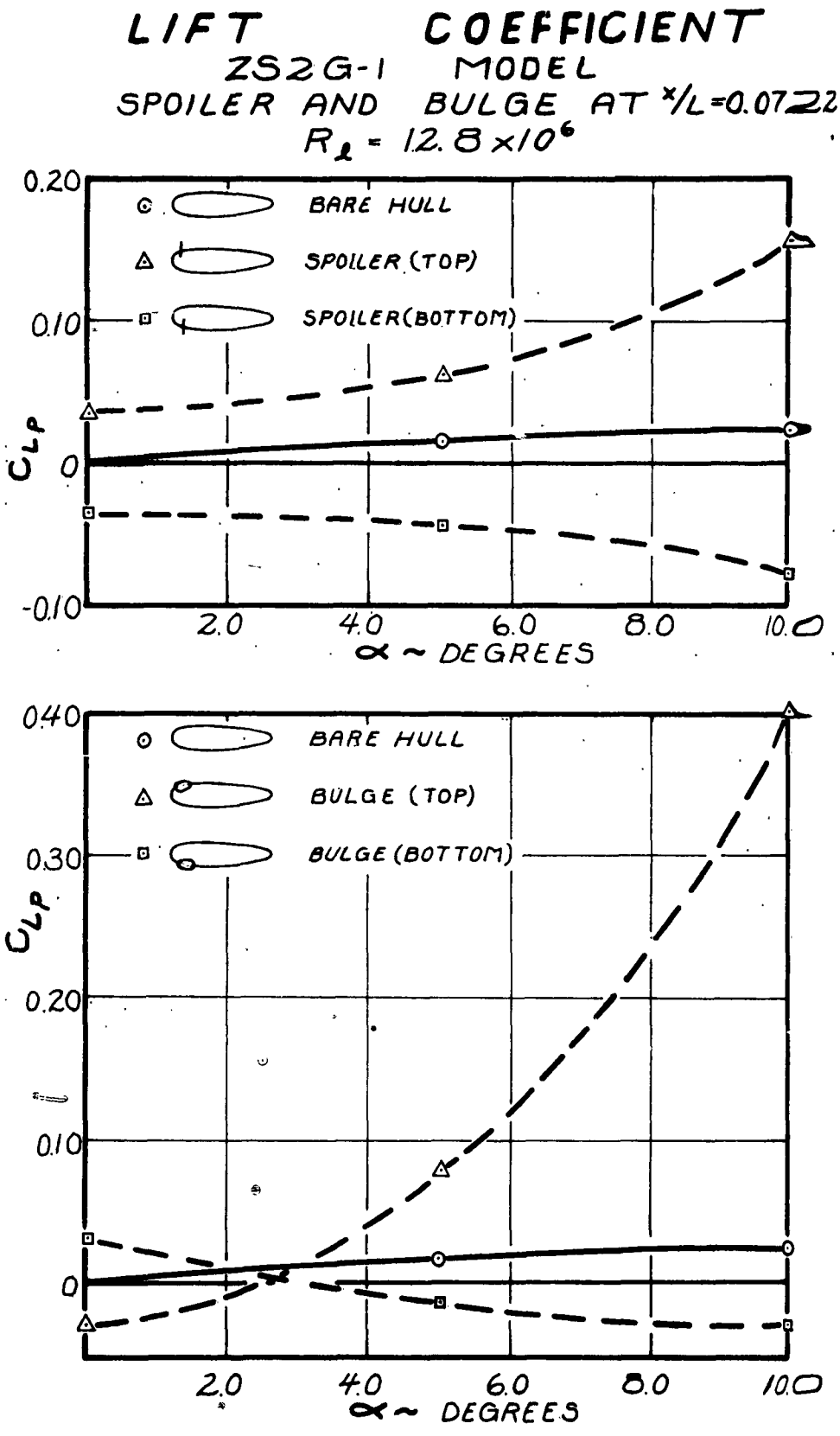
LIFT COEFFICIENT
ZS2G-1 MODEL
SPOILER AND BULGE AT x/L=0.0722
$R_\ell = 12.8 \times 10^6$
BARE HULL
SPOILER (TOP)
SPOILER (BOTTOM)
C_{LP}
0.20
0.10
0
-0.10
2.0
4.0
6.0
8.0
10.0
α ~ DEGREES
BARE HULL
BULGE (TOP)
BULGE (BOTTOM)
C_{LP}
0.40
0.30
0.20
0.10
0
2.0
4.0
6.0
8.0
10.0
α ~ DEGREES

FIGURE 13

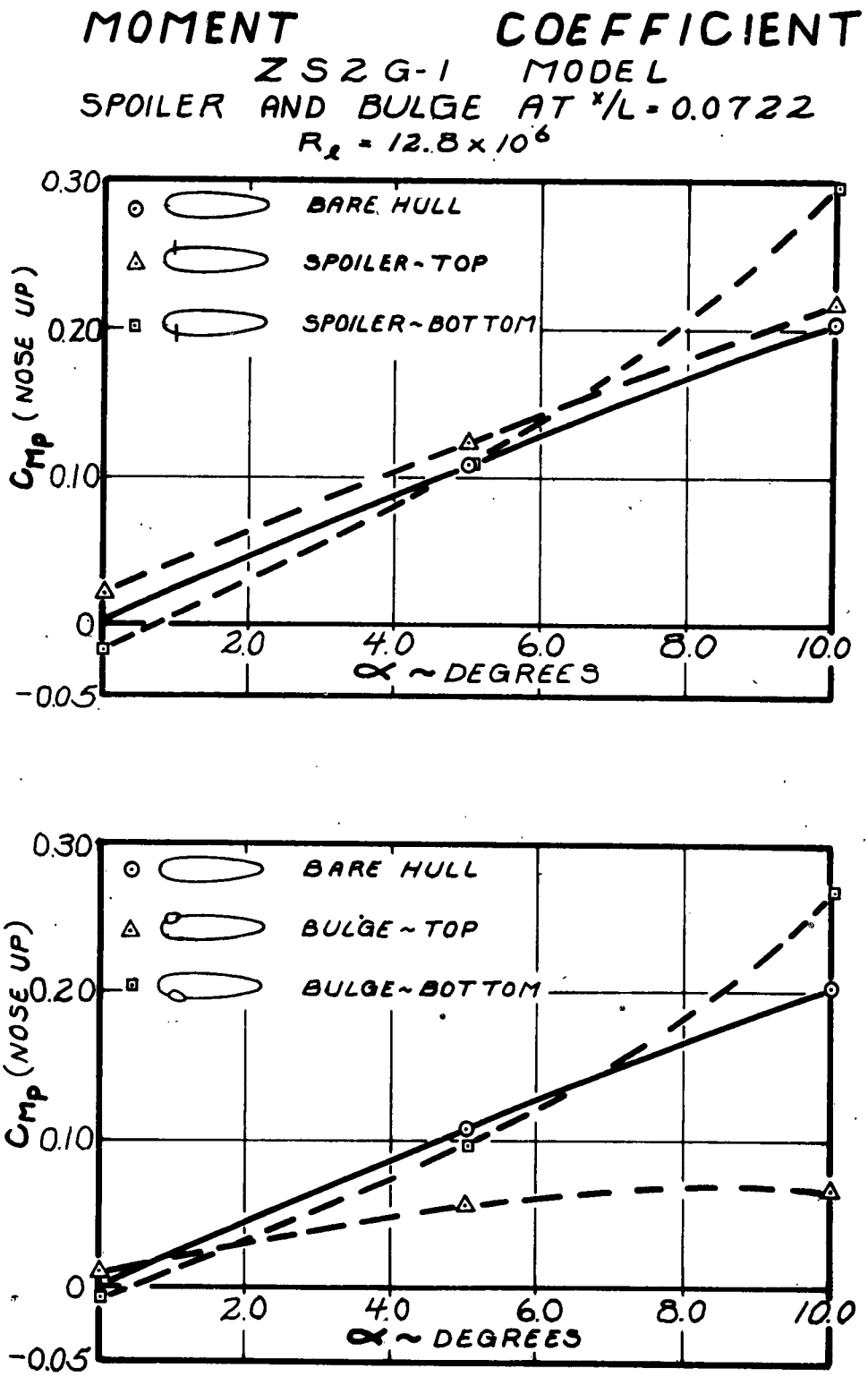
MOMENT COEFFICIENT
ZS2G-1 MODEL
SPOILER AND BULGE AT x/L = 0.0722
$R_\ell = 12.8 \times 10^6$
BARE HULL
SPOILER-TOP
SPOILER-BOTTOM
BULGE-TOP
BULGE-BOTTOM
C_{M_p} (NOSE UP)
0.30
0.20
0.10
0
-0.05
2.0
4.0
6.0
8.0
10.0
α ~ DEGREES

ESTIMATED MOMENT COEFFICIENT AVAILABLE FROM STERN ROTOR AT 15° TILT

ADVANCED ZSG-1 AIRSHIP

U_{MAX} = 100 KNOTS AT $\alpha = 0°$

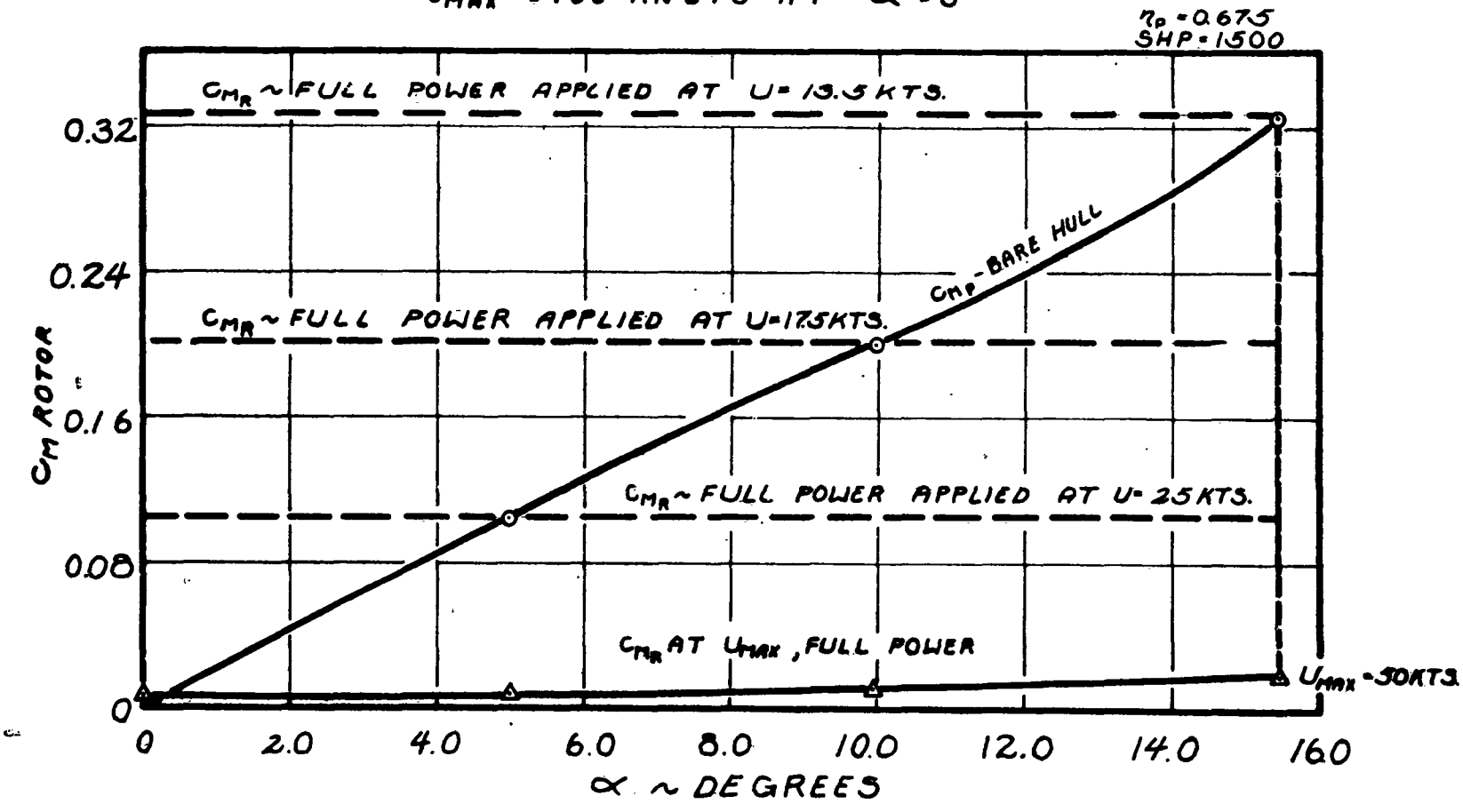

FIGURE 14

FIGURE 15

MOMENT COEFFICIENT FOR ADVANCED ZS2G-1 AIRSHIP WITH ROTOR AND BULGE ARRANGEMENT

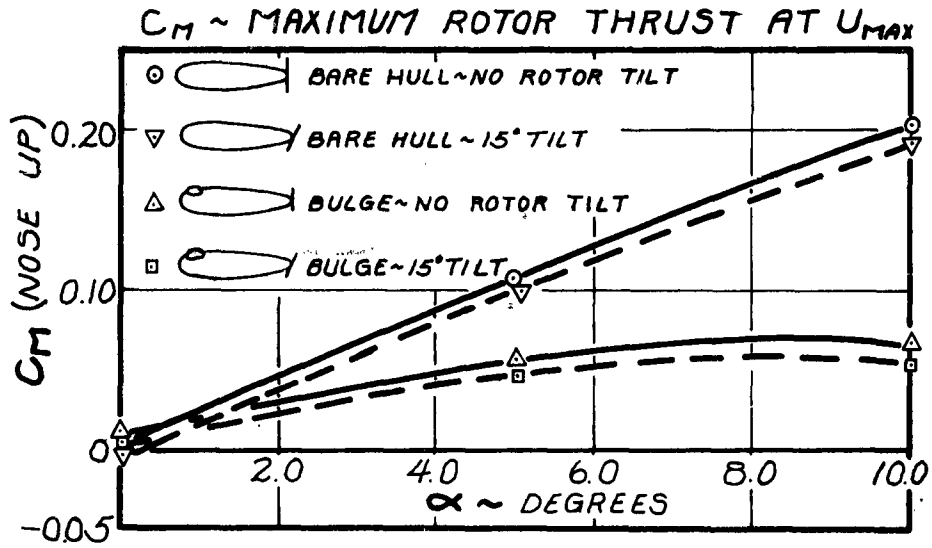

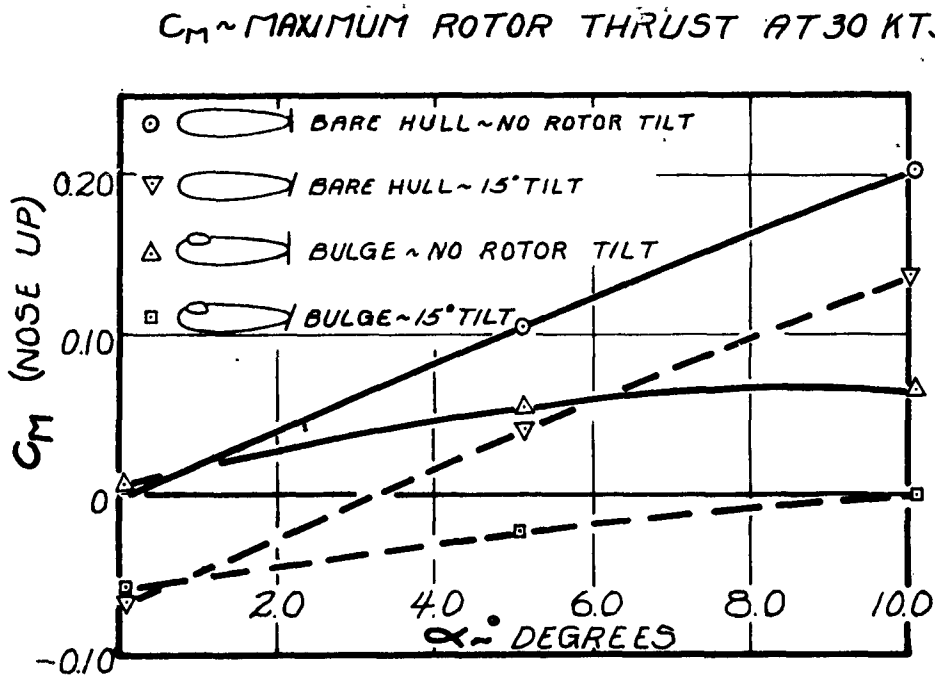

FIGURE 16

COMPARISON OF MOMENT COEFFICIENTS OF ADVANCED AND ORIGINAL AIRSHIP CONFIGURATIONS

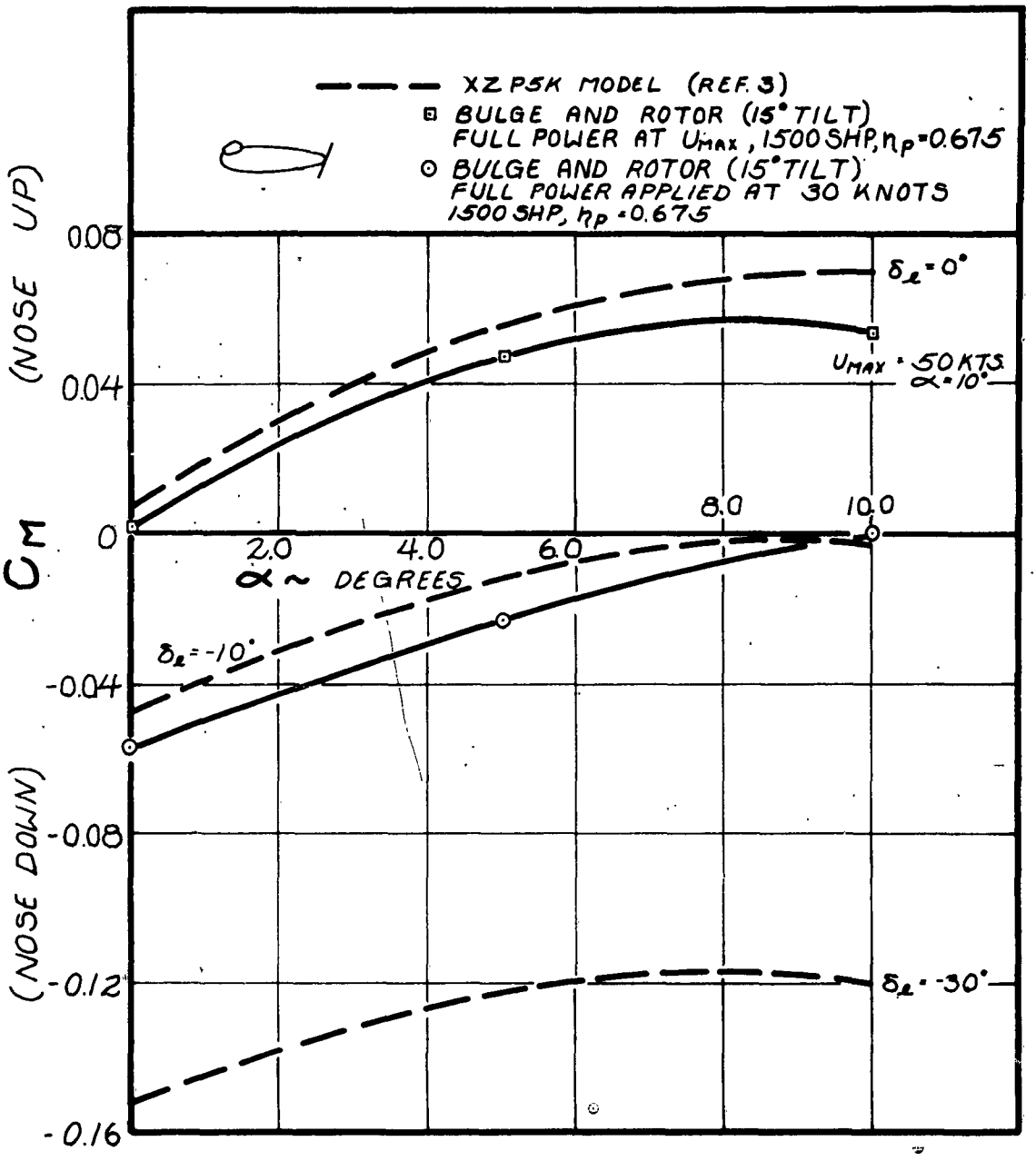

Aerophysics Department, Mississippi State University

Distribution List for Research Report #36

Under Contract Nonr 978 (02)

DEPARTMENT OF THE NAVY:

Chief, Bureau of Naval Weapons (RAAD-3)
Department of the Navy
Washington 25, D. C. 3 Copies

Chief, Bureau of Naval Weapons (DLI-3)
Department of the Navy
Washington 25, D. C. 2 Copies

Chief, Bureau of Naval Weapons (RA-7)
Department of the Navy
Washington 25, D. C. 1 Copy

Chief, Bureau of Naval Weapons (RRRE)
Department of the Navy
Washington 25, D. C. 1 Copy

Chief, Bureau of Naval Weapons (RRSY-5)
Department of the Navy
Washington 25, D. C. 1 Copy

Chief, Bureau of Naval Weapons (GM)
Department of the Navy
Washington 25, D. C. 2 Copies

Commanding Office & Director
David Taylor Model Basin
Aerodynamics Laboratory
Washington 7, D. C. 2 Copies

Commanding Office & Director
David Taylor Model Basin
Hydromechanics Laboratory
Washington 7, D. C. 2 Copies

Commander
U. S. Naval Ordance Laboratory
Aeronautical Mechanics Division
Silver Springs 19, Maryland
Attn: Dr. Kurzweg 1 Copy

Chief of Naval Research (Code 461)
Department of the Navy
Washington 25, D. C. 10 Copies

Chief of Naval Research (Code 429)
Department of the Navy
Washington 25, D. C. 1 Copy

Chief of Naval Research (Code 438)
Department of the Navy
Washington 25, D. C. 1 Copy

Commanding Officer
Office of Naval Research Branch Office
The John Crerar Library Building
86 E. Randolph Street
Chicago 1, Illinois 1 Copy

Commanding Officer
Office of Naval Research Branch Office
Navy #100 Fleet Post Office
New York, New York 2 Copies

Commanding Officer
Officer of Naval Research Branch Office
346 Broadway
New York 13, New York 1 Copy

Commanding Officer
Office of Naval Research Branch Office
1000 Geary Street
San Francisco 9, California 1 Copy

Commanding Office
Office of Naval Research Branch Office
495 Summer Street
Boston 10, Massachusetts 1 Copy

Commanding Officer
Office of Naval Research Branch Office
1030 E. Green Street
Pasadena, California 1 Copy

Contract Administrator
Southeastern Area
Office of Naval Research
2110 G Street, N. W.
Washington 7, D. C. 1 Copy

Director
Naval Research Laboratory
Technical Information Office
Washington 25, D. C. 6 Copies

Chief, Bureau of Ships (Code 421)
Department of the Navy
Washington 25, D. C 1 Copy

Assistant Chief for Research & Development
(Code 335)
Technical Information Branch
Bureau of Ships
Department of the Navy
Washington 25, D. C. 1 Copy

Research and Development Warfare Systems
Division (Code 361)
Anti-submarine Warfare Branch
Bureau of Ships
Department of the Navy
Washington 25, D. C. 1 Copy

Assistant Chief for Design Ship Building
(Code 440)
Ship Design Division (Hull)
Bureau of Ships
Department of the Navy
Washington 25, D. C. 1 Copy

Assistant Chief for Design Shipbuilding
(Code 525)
Ships Division, Submarines
Bureau of Ships
Department of the Navy
Washington 25, D. C. 1 Copy

Commanding Office & Director
David Taylor Model Basin
Hydrodynamics Laboratory
Washington 7, D. C. 1 Copy

DEPARTMENT OF THE AIR FORCE:

Commander
Air Research & Development Command
U. S. Air Force
Andrews Air Force Base
Washington 25, D. C. 1 Copy

Air Research & Development Command
U. S. Air Force
Office of Scientific Research
Washington 25, D. C. 1 Copy

Headquarters
Air Research & Development Command
Detachment One
Directorate of Systems Management
Wright-Patterson Air Force Base,
Ohio, Attn: RDZSC 1 Copy

Commander
Wright Air Development Center
Aeronautical Research Laboratory
Wright-Patterson Air Force Base,
Ohio 1 Copy

OTHER GOVERNMENT AGENCIES:

Commander
Armed Services Technical Information
Agency
Document Service Center
Arlington Hall Station
Arlington 12, Virginia 10 Copies

National Aeronautics & Space
Administration
Langley Research Center
Langley Air Force Base, Virginia
Attn: Mr. Donnelly 1 Copy

National Aeronautics & Space
Administration
Headquarters
1512 H Street, N. W.
Washington 25, D. C.
Attn: Mr. R. May 2 Copies

UNIVERSITIES:

Cornell University
Graduate School of Aeronautics
Ithaca, New York
Attn: Dr. W. R. Sears 1 Copy

The John Hopkins University
Applied Physics Laboratory
Baltimore 18, Maryland
Attn: Dr. F. H. Clauser,
Dr. D. W. Rabenhorst 1 Copy

Massachusetts Institute of Technology
Aeronautical Engineering Department
Cambridge 30, Massachusetts
Attn: Dr. R. H. Miller 1 Copy

Naval Postgraduate School
Aeronautical Engineering Department
Monterey, California
Attn: Dr. R. Head 1 Copy

Stevens Institute of Technology
Fluid Dynamics Laboratory
Hoboken, New Jersey
Attn: Mr. L. H. Mott 1 Copy

CORPORATIONS & INDUSTRIAL LABORATORIES:

Aerojet Engineering Corporation
Aerojet-General Corporation
Azusa, California
Attn: Mr. W. House 1 Copy

Goodyear Aircraft Corporation
1210 Massillon Road
Akron 15, Ohio 1 Copy

Grumman Aircraft Engineering Corp.
Bethpage, L. I., New York
Attn: Dr. C. E. Mack, Chief of Research
Mr. F. T. Kurt 1 Copy

Electric Boat Company
Division of General Dynamic Corp.
Groton, Connecticut 1 Copy